Temperature characterization in the collection tank of the NIST 26 m³ *PVTt* gas flow standard

Aaron N Johnson, John D Wright, Michael R Moldover and Pedro I Espina

National Institute of Standards and Technology, 100 Bureau Drive, Stop 8361, Gaithersburg, MD 20899-8361, USA

E-mail: aaron.johnson@nist.gov

Abstract
Gas temperature gradients created during the filling stage of a pressure–volume–temperature–time (*PVTt*) calibration cycle, and those imposed by inhomogeneous room conditions, lead to uncertainties in the average gas temperature in the collection tank. Because these temperature uncertainties dominate the overall flow uncertainty, NIST upgraded the temperature-averaging scheme used in its 26 m³ *PVTt* system. Instead of arithmetically averaging 10 thermistors to obtain the mean gas temperature, we now calculate this value via a volume-weighted trapezoidal integration procedure using 35 thermistors. Applying the new temperature-averaging scheme, the mean gas temperature can be determined with a standard uncertainty of 89 mK after only 2700 s of fan mixing. As a result, the flow uncertainty in the NIST 26 m³ *PVTt* system has decreased from 0.22% to 0.13% (with a coverage factor of 2). This paper highlights the temperature improvements and presents a detailed analysis for estimating the lower temperature uncertainty.

1. Introduction

The NIST 26 m³ pressure–volume–temperature–time (*PVTt*) flow calibration system is the USA primary standard for measuring gas flow from $0.017\,\text{kg s}^{-1}$ to $1.56\,\text{kg s}^{-1}$ at line pressures between 200 kPa and 700 kPa. The system is schematically shown in figure 1, and its main components are a steady source of flow (usually dry filtered air at room temperature), a critical flow venturi, bypass and tank inlet valves, an inventory volume and a collection tank. Additional components not shown include the pressure and temperature instrumentation, and the timing apparatus.

The overall mass flow uncertainty for *PVTt* systems derives from measurements of time, the inventory volume and its average gas density, and the collection tank volume and its average gas density. Both the collection tank and inventory volume gas densities must be determined twice during a flow measurement cycle. The average gas density in the collection tank is initially determined while the collection tank is evacuated, and again after the tank has been pressurized
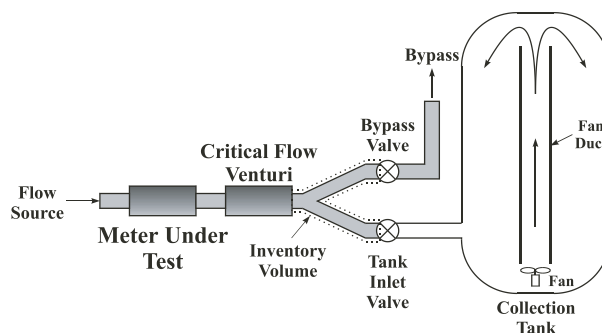
Figure 1. Schematic diagram of the NIST 26 m³ *PVTt* gas flow standard.

to 1 atm. Similarly, the average gas density in the inventory volume is also measured twice, during the initial diversion process that directs flow into the collection tank and again during the final diversion process.

Figure 2 illustrates the percentage contribution of each component to the mass flow uncertainty for the NIST *PVTt*
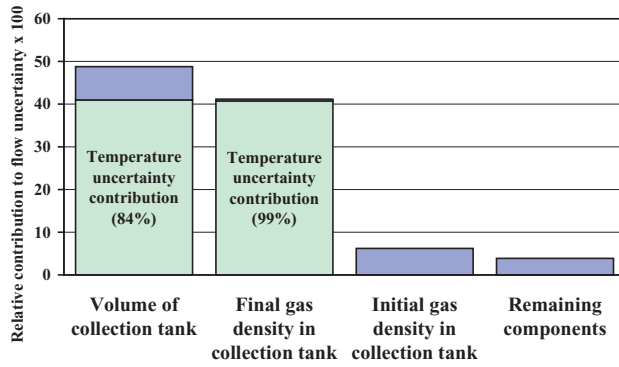
Figure 2. Contribution of density, volume and time measurements to the overall flow uncertainty of the NIST 26 m^3 *PVTt* gas flow standard.

system. The smallest uncertainty components represent only 4% of the total flow uncertainty and are grouped under the heading *remaining components* (i.e. the size of the inventory volume, the initial and final average gas densities in the inventory volume, and the cycle time measurement). The largest components derive from measurements of the collection tank volume and the final average gas density in the collection tank; together, these components amount to 90% of the mass flow uncertainty. This paper focuses on reducing the larger uncertainties due to determining the average gas density and the tank volume by improving the temperature uncertainty.

The measurement uncertainty of both the collection tank volume and the final average gas density are predominantly caused by uncertainties in determining the average temperature of the gas in the collection tank. The average gas temperature directly affects the average gas density via the equation of state. Likewise, the average temperature indirectly affects collection volume measurements via a gravimetric weighing procedure used for its determination [1]. As seen in figure 2, the uncertainty in the average gas temperature accounts for 84% of the uncertainty in the collection tank volume and comprises 99% of the uncertainty in the final average gas density. (These percentages are based on an estimated average gas temperature uncertainty of 210 mK that existed prior to this work.)

The predominant source of uncertainty in the average gas temperature results from spatial temperature variations of the gas inside the collection tank. These temperature inhomogeneities derive from two sources: (1) inhomogeneities imposed on the gas from temperature gradients in the room surrounding the collection tank; and (2) residual temperature inhomogeneities remaining in the collected gas resulting from the evacuation and filling processes of a flow measurement cycle. Given sufficient time, the temperature gradients in the gas caused by the calibration cycle decay; however, the gradients imposed by the room persist.

In order to reduce the stabilization time and decrease temperature non-uniformities in the gas, NIST has traditionally mixed the collected gas using a ducted fan as shown in figure 1. In 1971, Olsen and Baumgarten [2] estimated that fan mixing reduced the maximum temperature difference in the gas to ≈100 mK. However, this was never verified by a detailed study. Moreover, since temperature inhomogeneities imposed by the room have been observed to change seasonally with the

room heating and cooling system, it is not clear that this value is valid year round. In fact, several months of temperature measurements indicated that temperature differences on the surface of the collection tank range from 0 K to 2 K along its height and from 100 mK to 400 mK along its circumference. Measurements of temperature in the gas revealed differences in excess of 100 mK near the fan motor and in the thermal boundary layer adjacent to the tank wall.

In the past, the average gas temperature was determined by the arithmetic average of 10 thermistors [3]. We estimate that this averaging procedure yields uncertainties due to spatial non-uniformities of 200 mK (with a unity coverage factor). In this work, we characterized the average gas temperature using an array of 35 thermistors and computed the average temperature using a trapezoidal integration rule [4]. Several thermistor configurations were tested to determine the optimal thermistor placement. Using the new approach, the average gas temperature is now computed to a standard uncertainty of 89 mK (with a unity coverage factor), more than 100 mK less than the previous approach. The lower temperature uncertainty has reduced the mass flow measurement uncertainty from 0.22% to 0.13% (with a coverage factor of 2).

2. Principle of operation

The *PVTt* system measures flow using a volumetric timed-collection technique, whereby a steady flow is diverted into a nearly empty collection tank of known volume for a measured time interval. The average gas temperature and pressure in the tank are measured before and after the filling process. These measurements are used to determine the density change in the collection volume attributed to the filling process. In principle, the mass flow can be determined by multiplying the density change by the collection vessel volume, and dividing the result by the collection time. The final equation for mass flow in the *PVTt* system includes a correction term for the mass changes occurring in the inventory volume and is given by

$$\dot{m} = \frac{(\rho_T^f - \rho_T^i)V_T + (\rho_I^f - \rho_I^i)V_I}{\Delta t} \qquad (1)$$

where ρ_T^f is the collection tank final average density, ρ_T^i is the collection tank initial average density, V_T is the collection tank volume, ρ_I^f is the inventory volume final average density, ρ_I^i is the inventory volume initial average density, V_I is the inventory volume and Δt is the gas collection time interval.

3. Time record of *PVTt* flow measurement cycle

Figure 3 shows temperature and pressure time traces for a typical *PVTt* flow measurement cycle. In the figure, times less than zero correspond to the emptying and filling of the collection tank, whereas times greater than zero correspond to the temperature and pressure stabilization period. The average gas pressure is plotted on the right *y*-axis while the average gas temperature, the average tank surface temperature and the fan duct temperature (see figure 1) are plotted on the left *y*-axis.

Before emptying the collection tank, the average gas pressure and temperature are near room conditions. While the
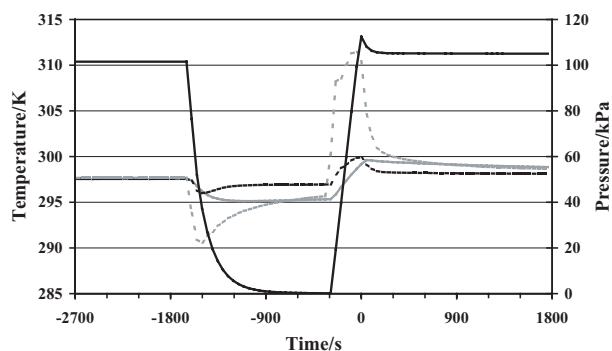
Figure 3. Pressure and temperature time traces for a typical *PVTt* calibration cycle.

Figure 4. Schematic of internal geometry of the NIST 26 m³ *PVTt* tank.

collection tank is emptying, both the average gas pressure and temperature decrease. During the filling process, flow work phenomena [5] cause the average gas temperature to increase by as much as 25 K. The warm gas heats both the surface of the collection tank and the fan duct, causing their temperatures to increase by as much as 2.5 K and 5 K, respectively. Moreover, all of the temperature traces shown in figure 3 are spatially averaged quantities, but the actual gas temperature distribution is inhomogeneous and spans as much as 30 K just after filling. This paper focuses on determining the required stabilization time and an appropriate configuration of thermistors that will yield low uncertainty average gas temperature measurements.

4. Temperature characterization

Figure 4 shows both vertical and horizontal cross-sections of the collection tank and fan duct geometry. The collection tank is made from 1.3 cm thick carbon steel and has a height of 4.88 m and maximum diameter of 2.74 m. The fan duct has a diameter of 30.5 cm and is also made of carbon steel. The height of the fan duct is 3.7 m and its thickness is 1 cm. The fan duct is supported by five tiers of radial arms spaced vertically 92 cm apart. Each tier has five radial arms spaced 72° apart that support the thermistors. At the base of the fan duct, a $0.24 \, \mathrm{m}^3 \, \mathrm{s}^{-1}$ fan is used to mix the gas. In the remaining sections we characterize the temperature distribution in the gas. In addition, we measure the temperature profile on the collection tank walls, on the fan duct and on the radial supports, and assess their effect on the average gas temperature.

4.1. Temperature measurements on the collection tank surface

The exterior surface temperature of the collection tank was measured before and during the flow measurement cycle using an array of thermocouples. Before the calibration cycle, the temperature was vertically stratified. The magnitude of the vertical gradient changed from day to day, depending on the operation of the room heating system. Typically, the top of the tank was 800 mK warmer than its bottom. In the worst case recorded, the top was 2 K warmer than the bottom. In comparison, the angular temperature differences along the exterior surface of the tank were much smaller, ranging from 100 mK to 400 mK.

The emptying and the filling processes altered the temperature profiles on the surface of the collection tank.
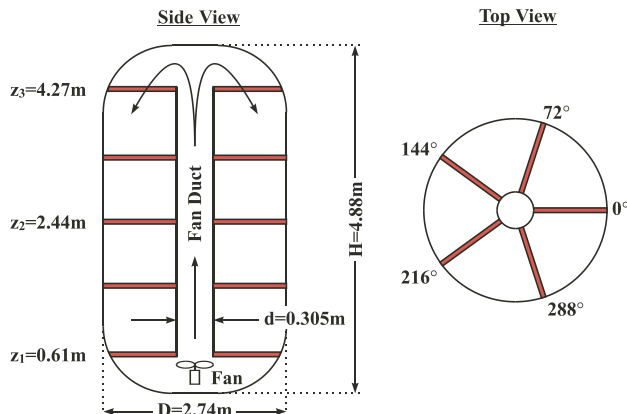
Just after filling the tank, angular temperature differences were as large as 1 K and vertical differences were as large as 3.5 K. With the fan on, these temperature differences approached their original values in ≈2700 s. After this time, the remaining gradients were predominantly due to the temperature inhomogeneity that existed on the collection tank before the calibration cycle started.

4.2. Temperature measurements on the fan duct and radial supports

The 5 K increase in the fan duct temperature that occurs just after filling was measured using three thermistors positioned at $z_1 = 0.61$ m, $z_2 = 2.44$ m and $z_3 = 4.27$ m, as shown in figure 4. With the fan off, temperature differences of this magnitude persisted for several hours. With the fan on, the airflow through the duct has a Reynolds number of ≈60 000 and the resulting turbulent convective heat transfer reduced temperature differences along the duct to less than 200 mK within 3600 s. The flow driven by the fan also dissipated the heat stored in the radial supports. Just after filling, one radial support was 3 K warmer than the surrounding gas. This difference decreased to less than 50 mK after 2700 s of fan mixing.

Heat dissipated by the 55 W fan motor at the base of the fan duct creates a local hot zone. The hot zone extends radially outward from the base of fan duct ≈20 cm, and upward ≈50 cm. The temperature difference in this zone was ≈500 mK after 1800 s of fan mixing. The volume of the hot zone is only 0.6% of the volume of the tank, so that its contribution to the uncertainty of the average gas temperature is less than 3 mK.

4.3. Thermal boundary layer measurements

The thickness of the internal thermal boundary layer was measured along the lateral section of the collection tank wall at two heights, $z_1 = 0.61$ m and $z_3 = 4.27$ m (see figure 4). At both heights, the temperature profile was measured using 13 thermistors distributed radially at $\theta = 0°$. To resolve the thermal boundary layer, eight of these thermistors were located at 0 cm, 1 cm, 2 cm, 3 cm, 5 cm, 7 cm, 10 cm and 20 cm, respectively. The remaining five thermistors were uniformly spaced 20 cm apart across the remainder of the radius.

During the initial stages of the temperature stabilization period, the heat transfer through the thermal boundary layer is governed by turbulent natural convection from the warm gas to the cooler tank wall. As the gas temperature drops, natural convection diminishes. With the fan off, the gas temperature requires several hours to return to the stratified temperature distribution imposed by the tank surface. Although the temperature stabilization time is reduced by using the fan to mix the gas, the heat generated by the fan motor maintains a slight temperature difference between the bulk of the gas and the tank surface. This temperature difference results in a thermal boundary layer adjacent to the tank wall whose thickness is predominantly governed by the flow patterns produced by the fan. Gas emanating from the top of the fan duct flows downward in the collection tank (see figure 4), forming a boundary layer along the tank's lateral surface. The velocity of the downward flow is approximately $u = Q_{fan}/A_{cs} = 0.04\,\mathrm{m\,s^{-1}}$, where Q_{fan} is the volumetric flow produced by the fan, and $A_{cs} = \pi(D^2 - d^2)/4$ is the cross-sectional flow area. The Reynolds number at lowest elevation ($z_1 = 0.61\,\mathrm{m}$ plane) is ≈ 9000 so that the thermal boundary layer is fully laminar and its thickness at various heights can be estimated from the Blasius similarity solution for laminar flow over a flat plate [6],

$$\delta_{\mathrm{T}}(z) = 5(z_3 - z)Pr^{-1/3}Re^{-1/2} \qquad (2)$$

where Pr is the Prandtl number and Re is the local Reynolds number. Based on this theory, the maximum thickness of the thermal boundary layer, $\delta_{\mathrm{T}}(z_1) = 21\,\mathrm{cm}$, occurs at the $z_1 = 0.61\,\mathrm{m}$ elevation. This predicted value agrees well with the measured boundary layer thickness at this location of nominally 20 cm. As expected, the measured boundary layer thickness was thinner near the top of the tank, $\delta_{\mathrm{T}}(z_3) = 2\,\mathrm{cm}$.

Boundary layer temperature measurements were taken for varying degrees of stratification on the tank surface over a period of several months. The uncertainty due to temperature gradients in the thermal boundary layer was estimated by multiplying the fraction of volume occupied by the boundary layer by the average temperature difference across the boundary layer. Assuming the boundary layer develops according to the Blasius flat plate profile, the boundary layer region will occupy $\approx 20\%$ of the tank volume. Because the steepest temperature gradients were caused by turbulent natural convection and occurred closer to the wall than those predicted by the Blasius temperature distribution, the estimated volume fraction is a conservative upper bound of the boundary layer region.

The average temperature difference across the boundary layer, $\langle \Delta T_{\mathrm{BL}} \rangle$, is calculated by a weighted average of the local temperature difference over the entire boundary layer region

$$\langle \Delta T_{\mathrm{BL}} \rangle = \frac{1}{V_{\mathrm{BL}}} \int_{V_{\mathrm{BL}}} (T_{\mathrm{w}} - T_{\infty}) f(\eta)\, \mathrm{d}V \qquad (3)$$

where V_{BL} is the volume occupied by the boundary layer, T_{w} is the local wall temperature, T_{∞} is the local temperature in the region outside the boundary layer (i.e. the far-field) and $f(\eta)$ is a second-degree curve fit to the Blasius thermal boundary layer similarity function [6]. Here, $\eta = r/\delta_{\mathrm{T}}$ is the scaled distance measured from the wall, and the temperature difference between the wall and the far-field, $(T_{\mathrm{w}} - T_{\infty})$, is

assumed to vary linearly between the two measured values at $z_1 = 0.61\,\mathrm{m}$ and $z_3 = 4.27\,\mathrm{m}$. Boundary layer temperature measurements at the $z_1 = 0.61\,\mathrm{m}$ elevation showed reasonable agreement with this similarity temperature profile.

The average temperature difference across the boundary layer, $\langle \Delta T_{\mathrm{BL}} \rangle$, varied from day to day, changing with the degree of temperature stratification on the collection tank. In the worst case measured, the average temperature difference across the thermal boundary layer was $\langle \Delta T_{\mathrm{BL}} \rangle = 250\,\mathrm{mK}$, which when multiplied by the volume fraction occupied by the boundary layer (0.2) yields a 50 mK uncertainty in the average temperature of the gas in the collection tank.

4.4. Temperature measurements in the far-field

The vertical temperature stratification in the gas posed the greatest problem in determining the average gas temperature in the far-field. To adequately resolve these vertical temperature gradients, the average gas temperature was determined by an array of 35 thermistors distributed in a vertical plane between $z_1 = 0.61\,\mathrm{m}$ and $z_3 = 4.27\,\mathrm{m}$ at $\theta = 0°$ (see figure 4). Seven thermistors were uniformly spaced in the vertical direction, and five thermistors were uniformly spaced in the radial direction[1] with the first thermistor located 12 cm from the fan duct and the fifth thermistor positioned 13 cm from the collection tank surface. The average gas temperature, $\langle T \rangle$, was calculated at various times during the temperature stabilization period. Table 1 shows $\langle T \rangle$ at 1800 s, 2700 s, 3600 s, 5400 s, 7200 s and 14 400 s. At each time, the average temperature was determined twice, once using all 35 sensors, and again using only 14 of the 35 thermistors. The configuration with 14 sensors used only the two outermost sensors in the radial direction at each of the seven vertical elevations.

Sampling or discretization errors will affect the accuracy of the calculated average gas temperature. The magnitude of these errors depends on the number of thermistors used to characterize the far-field temperature profile. The size of this error should decrease when more thermistors are used. In an attempt to determine an upper bound of this error (for a fixed number of sensors), we defined a temperature error bound, ΔT. This error bound is calculated by (1) estimating the maximum *local* discretization error between adjacent thermistors, and (2) summing the local error from all of the thermistors. Here, the maximum local error is taken to be equal to $|\delta T|/2$ where δT is the temperature difference between two adjacent thermistors. Physically, this bound is consistent with the idea that the far-field temperature variations are either small or vary in a predictable manner. The validity of this assumption increases with longer stabilization times and with a larger number of sensors. In this work we estimated that the discretization error equalled $\langle T_{35} \rangle - \langle T_{14} \rangle$ (i.e., the difference in average temperatures using 35 versus 14 thermistors). Since the temperature error bound should be greater than or equal to the discretization error we expect that at all times $\Delta T \geqslant \langle T_{35} \rangle - \langle T_{14} \rangle$.

Table 1 highlights typical trends of the discretization error, $\langle T_{35} \rangle - \langle T_{14} \rangle$, as well as the temperature error bounds, ΔT_{35} and ΔT_{14}. During the first 3600 s of fan mixing, the

---

[1] Fishing line was added between the five radial arms to allow positioning of thermistors at any desired vertical or radial distance.

Table 1. Typical results of far-field temperature testing: average temperature, $\langle T \rangle$, and estimated error bound, ΔT, evaluated using 35 and 14 thermistors.

14 thermistors (2 × 7)			35 thermistors (5 × 7)		
Time/ s	$\langle T_{14} \rangle$/ K	ΔT_{14}/ mK	$\langle T_{35} \rangle$/ K	ΔT_{35}/ mK	$\langle T_{35} \rangle - \langle T_{14} \rangle$/ mK
1 800	296.279	34	296.300	40	21
2 700	296.168	22	296.173	17	5
3 600	296.120	21	296.111	11	−9
5 400	295.909	37	295.900	26	−9
7 200	295.817	38	295.806	26	−11
14 400	295.567	26	295.562	23	−5

Table 2. Uncertainty components for the average temperature.

Source	Magnitude/mK	Section
Temperature differences near the fan motor	3	4.2
Temperature differences in the thermal boundary layer	50	4.3
Temperature differences in the far-field	49	4.4
Thermistor calibration and drift between calibrations	54	4.5
Root sum squares	89	4.6

vertical and radial temperature gradients decreased, causing a corresponding decrease in $\langle T_{35} \rangle - \langle T_{14} \rangle$, ΔT_{35} and ΔT_{14}. After turning the fan off at 3600 s, the vertical gradients began to increase due to temperature stratification. The radial gradients near the fan motor also increased since heat removal via natural convection processes (with the fan off) was less effective than for forced convection processes (with the fan on). As a result of the larger temperature gradients, the discretization error increased from the time the fan was turned off until 7200 s into the stabilization period. At times greater than 7200 s the hot zone near the fan motor had cooled so that discretization reduced to previous levels just before the fan was turned off. However, ΔT_{35} and ΔT_{14} remained larger than corresponding values with the fan on due to vertical stratification in the far-field.

At first sight, it was surprising that $\Delta T_{35} > \Delta T_{14}$ at $t = 1800$ s. At this early time, the temperature non-uniformities created from the filling process were not completely dissipated. Nevertheless, the averages calculated with only 14 thermistors compared favourably with those calculated with 35 thermistors, having a maximum difference of only 21 mK. Moreover, the temperature difference between the two average temperatures, $\langle T_{35} \rangle - \langle T_{14} \rangle$, is well below the estimated discretization error, which gives us confidence that the estimated discretization error is a reasonable upper bound for the true error. The temperature uncertainty in the vertical direction is taken to be equal to the average temperature difference, $\langle T_{35} \rangle - \langle T_{14} \rangle$, which from table 1 at 2700 s has a magnitude of 5 mK.

Initially, the low temperature uncertainty of the vertical thermistor configuration was somewhat surprising. However, since the vertical temperature profile remains reasonably linear during fan mixing, the trapezoidal integration scheme yielded a nearly error-free result. Unfortunately, the vertical thermistor configuration did not account for angular temperature differences, which were found to be somewhat larger. The angular discretization error was estimated by temperature measurements that were made with all 35 sensors positioned at the $z_1 = 0.61$ m cross-section. These measurements showed azimuthal inhomogeneities of ≈ 10 mK near the fan duct and of 100 mK near the edge of the thermal boundary layer. Trapezoidal integration of this angular thermistor configuration indicated that the angular discretization error was nominally 62 mK after a 2700 s stabilization period. We expect that this value will be reduced in future work by repositioning the radially positioned thermistors into an angular orientation. The close agreement

between the calculated average temperatures, $\langle T_{14} \rangle$ and $\langle T_{35} \rangle$, in table 1 supports redistributing the thermistors in this manner.

The standard uncertainty for far-field temperature measurements (with a unity coverage factor) is determined by a root-sum-square of the vertical (5 mK) and angular (62 mK) temperature uncertainties at 2700 s into the stabilization period. The resulting uncertainty is 62 mK. When this value is multiplied by the 0.8 volume fraction of the far-field, the average temperature uncertainty in the far-field equals 49 mK.

4.5. Thermistor calibration and drift

The thermistors are calibrated in a nearly uniform temperature water bath using a thermistor transfer standard. The components of thermistor uncertainty resulting from this calibration include: 1 mK uncertainty from the PRT; 1 mK due to bath temperature non-uniformities; 3 mK due to thermistor self-heating, end conduction and radiation effects; 20 mK due to curve fit residuals; and 50 mK uncertainty for drift during the five-year scheduled calibration interval[2]. These components are root-sum-squared to obtain the total thermistor calibration uncertainty (54 mK).

4.6. Uncertainty of the average gas temperature

As summarized in table 2, the total temperature uncertainty was obtained by combining the thermistor calibration uncertainty with the temperature non-uniformity uncertainties using the root-sum-squared method [7]. This yielded an uncertainty of 89 mK at the 67% confidence level.

4.7. Temporal variations in the average density

While the local and average gas temperature can vary in time due to transient heat transfer conditions, conservation of mass requires that the average gas density remains time invariant. In figure 5, temporal variations in the computed average gas density are indicated as a percentage change. In this plot, $t = 21\,600$ s is taken to be infinity in the calculation of the percentage density change. The average gas density is determined from the average gas temperature and pressure via the equation of state. The average gas temperature shown in figure 5 resulted from a spatial average of the 35 thermistors arranged in the vertical configuration. However, essentially the same results were obtained when only 14 thermistors were

---

[2] The 50 mK attributed to drift is based on the specifications of the manufacturer; however, temperature control charts that monitor future calibrations might warrant reducing this value.
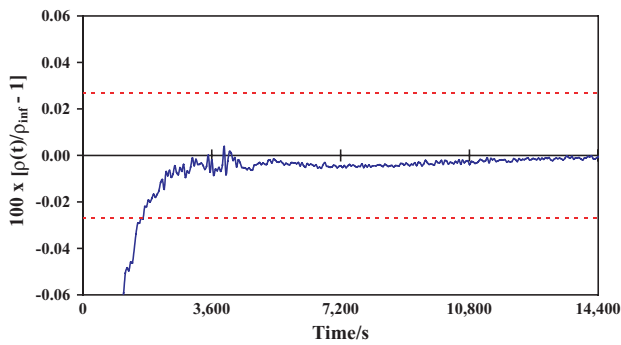
Figure 5. Change in the average gas density in the NIST 26 m³ *PVTt* tank during the stabilization period.

used (table 1, right column). The dashed lines in figure 5 represent the maximum and minimum density change due to the 89 mK temperature uncertainty.

Initially, the percentage change in the computed average density was large, but it decreased as temperature gradients from the emptying and filling processes subsided. After 1380 s of fan mixing, the density was within the 89 mK uncertainty tolerance indicated by the horizontal dashed lines. However, 2700 s of fan mixing was necessary for the density to stabilize. When the fan was turned off (3600 s into the stabilization period) the density did not change. This observation confirms our argument that the average is not significantly affected by the local heating near the fan motor or by the vertically stratified temperature profile that results when the fan is turned off. This result adds confidence that the temperature integration scheme adequately characterizes the average gas temperature.

5. Conclusions

An array of 35 thermistors was used to determine the average gas temperature in the collection tank of the NIST 26 m³ *PVTt* system during a flow measurement cycle. By arranging the thermistors in various configurations, the magnitude and decay rate of spatial temperature gradients was assessed. After 2700 s of fan mixing, the average temperature was determined with a standard uncertainty of 89 mK (unity coverage factor). The components of 89 mK are listed in table 2. The total temperature uncertainty of 89 mK is more than 100 mK less than previous estimates and it reduced the flow uncertainty from 0.22% to 0.13% (coverage factor of 2).

In the future we hope to further reduce the temperature uncertainty by modifying the thermistor configuration. The far-field temperature uncertainty of 49 mK primarily consisted of angular temperature non-uniformities. The average gas temperature in the far-field was determined using a trapezoidal integration scheme that averaged an array of sensors arranged in a vertical configuration. The integration was done for 14 and 35 thermistors arranged in a 2×7 array (two radial and seven vertical) and a 5×7 array. After 1800 s of fan mixing, the difference between the two sensor arrangements was less than 11 mK, and at larger times the difference became even smaller. Therefore, the 2×7 thermistor arrangement can be used to determine the average temperature without a significant loss of accuracy. Moreover, some of the sensors in the radial direction in the 5×7 thermistor arrangement can be placed into an angular orientation to reduce the estimated 62 mK uncertainty due to angular temperature gradients.

Acknowledgments

References

[1] Wright J D, Johnson A N and Moldover M R 2003 *J. Res. Natl Inst. Stand. Technol.* **108** 27–47
[2] Olson L and Baumgarten G 1971 *Flow: Its Measurement and Control in Science and Industry* (ISA) pp 1287–95
[3] Mattingly G E 1989 *NCSL Newsletter* **29** 1
[4] Press W H, Teukolsky S A, Vetterling W T and Flannery B P 2001 *Numerical Recipes in Fortran 77, The Art of Scientific Computing* (Cambridge: Cambridge University Press)
[5] Wright J D and Johnson A N 2000 *Proc. FLOMEKO 2000* (Salvador, Brazil: IPT 2000)
[6] White F M 1991 *Viscous Fluid Flow* 2nd edn (Singapore: McGraw-Hill)
[7] Coleman H W and Steele W G 1989 *Experimentation and Uncertainty Analysis for Engineers* (New York: Wiley)